Facet-Enhanced Dielectric Sensitivity in Plasmonic Metal Oxide Nanocubes

Benjamin J. Roman, Sofia A. Shubert-Zuleta, Grant Shim, Victoria Kyveryga, Mohamed Faris, and Delia J. Milliron*
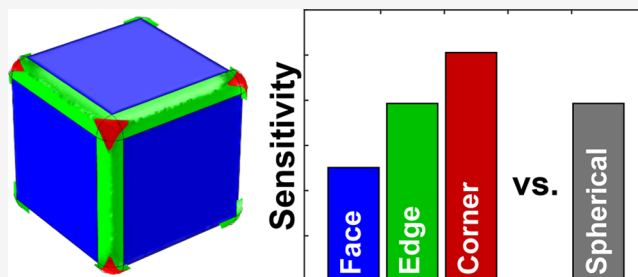
Read Online

ACCESS | Metrics & More | Article Recommendations | Supporting Information

ABSTRACT: The resonant frequency of plasmonic nanoparticles depends on the refractive index of the local environment, a property which is directly useful for sensing applications and is indicative of potential utility for other applications based on near-field enhancement of light intensity. While the morphology dependence of dielectric sensitivity has been well studied in noble-metal nanoparticles, less investigated is the sensitivity of degenerately doped metal oxide nanocrystals, whose plasmon resonances lie in the near- to mid-infrared region. Here, we report the dielectric sensitivity of fluorine and tin codoped indium oxide nanocubes and its dependence on their sharp faceting which gives rise to multiple plasmonic modes and on their tin-dopant concentration. We find that the plasmon mode associated with the nanocube corners is the most sensitive and that raising dopant concentration increases dielectric sensitivity. Comparing to finite element simulations that assume a spatially uniform free electron distribution in the nanocubes, we show that the plasmon modes associated with the edges and the faces of the nanocubes are less sensitive than expected and that their reduced dielectric sensitivity can be rationalized by the presence of band bending and a resulting surface depletion layer. Interestingly, simulations suggest that Fermi level pinning occurs predominantly on the cube faces, reshaping the free electron volume so that the depletion layer effectively insulates the faces and edges from the surrounding environment, while the corner mode remains sensitive.

INTRODUCTION

Plasmonic nanocrystals (NCs) have optical extinction spectra that depend not only on the material properties and NC morphology but also on the surrounding dielectric environment. This dielectric sensitivity has been widely explored for its applications in sensing, using shifts in the optical extinction to sensitively detect adsorbing molecules[1−3] and to monitor changes in adsorbed molecules, such as the binding of antibodies to bioactive proteins[4,5] or the shortening of adsorbed peptides due to enzyme-driven cleavage reactions.[6] The dielectric sensitivity is also an indication of how strongly the incident electromagnetic field is concentrated by the localized surface plasmon resonance (LSPR),[7] an effect that can be harnessed for surface-enhanced spectroscopies,[8,9] to drive chemical transformations through photothermal heating or hot electron generation[10−12] or to direct energy into molecular vibrational modes through resonant coupling.[13,14] As such, the shape and faceting of plasmonic NCs have been explored to increase their sensitivity by modifying the LSPR and its associated near-field enhancement (NFE); however, these studies have largely been restricted to noble-metal nanoparticles.[15−21]
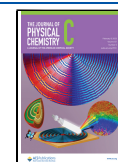
Less well studied is the sensitivity of degenerately doped metal oxide NCs, which are of particular interest for their tunable LSPR in the near- to mid-infrared (IR) spectral regions.[22,23] These materials, including the prototypical tin-doped indium oxide (ITO), are wide-bandgap semiconductors that are aliovalently doped such that their Fermi level lies above their conduction band minimum, and they behave as degenerate metals. As the free electron concentration of metal oxide NCs depends on the incorporated dopant density, their LSPR can be widely tuned across the IR while maintaining a consistent NC size and morphology.[22,24,25] Conversely, substantial tuning of the LSPR of noble-metal nanoparticles usually requires changing the particle size or morphology. In addition, while some noble-metal nanoparticle morphologies exhibit plasmonic properties in the IR region,[20,26−28] metal oxide nanostructures can have reduced long-range coupling and thus can be packed densely, maximizing the NFE hot spots at the ensemble level most relevant for sensing and enhanced spectroscopies.[9,14]

As with noble metals, particle shape plays a role in determining the LSPR spectra and near-field properties of metal oxide NCs.[29] Fluorine codoping leads to faceting of ITO, generating a cubic NC morphology.[25] The LSPR spectra of fluorine and tin codoped indium oxide (FITO) NCs have multimodal line shapes with three dipolar eigenmodes—one each associated with the corners, edges, and faces of the cube. The facets on NC cubes composed of indium-doped cadmium oxide, another degenerately doped plasmonic metal oxide material, were predicted by finite element simulations to increase NFE, with the strongest enhancement projected to occur around the corners and edges, additionally enhancing coupling between pairs of adjacent nanocubes.[29] In dense monolayer films of FITO nanocubes, strong NFE has been shown experimentally and theoretically to give rise to strong coupling between NC LSPR modes and molecular vibrational modes of surface-adsorbed molecules.[14]

On the other hand, the NFE around ITO NCs and the dielectric sensitivity of their LSPR are known to be reduced by the presence of a surface depletion layer which insulates the plasmonic volume from its local environment.[30] Fermi level pinning by surface states in the ITO band gap is responsible for the formation of the depletion layer.[31] The surface chemistry of fluorine-doped indium oxide NCs, however, is known to differ from ITO.[32] Fluorine doping in metal oxides also generally reduces plasmonic damping, which should boost both dielectric sensitivity and NFE.[25,32−34] Therefore, it is currently unknown the extent to which surface depletion impacts FITO NCs, how sensitive the FITO LSPR modes are to their local dielectric environment, and whether the faceting of FITO nanocubes improves their LSPR dielectric sensitivity.

In this work, we examine the dielectric sensitivity of FITO nanocubes, tracking the frequency shifts of each of the three geometric modes and their dependence on the at. % of Sn doping in the NCs. We find that the most intense LSPR mode, associated with the cube corners, is also the most sensitive. Additionally, through comparison with simulation, we find that the edge and face modes are less sensitive than expected for a spatially uniform dielectric function within the cube, especially for samples with lower Sn at. %. While the edge and face modes are less sensitive to changes in the dielectric environment, they shift *more* than the corner mode when electrons are added to the NCs using reductive chemical titrations. Both observations are consistent with surface depletion impacting the face and edge modes more severely than the corner mode. By simulating different surface Fermi level pinning scenarios, we show that the mode-dependent impact of surface depletion is best explained by Fermi level pinning occurring dominantly at the faces of the nanocubes.

■ MATERIALS AND METHODS

Materials. All chemicals were acquired commercially and were used as received, without any further purification. Indium(III) acetate [In(ac)$_3$, 99.99%, Sigma-Aldrich], tin(IV) acetate [Sn(ac)$_4$, Sigma-Aldrich], oleic acid (90%, technical grade, Sigma-Aldrich), oleyl alcohol (85%, technical grade, Sigma-Aldrich), and tin(IV) fluoride (SnF$_4$, 99%, Alfa Aesar) were used to synthesize the NCs. Hexane (≥99.9%, Fischer Chemical), ethanol (90%, Fischer Chemical), tetrachloro-ethylene (99%, Sigma-Aldrich), tetrahydrofuran (≥99.9%, Sigma-Aldrich), toluene (99.8%, Sigma-Aldrich), and chloro-form were used for the purification and characterization of NCs. For chemical reduction, decamethylcobaltocene, sodium

tetrakis[3,5-bis(trifluoromethyl)phenyl]borate, and bis-(pentamethylcyclopentadienyl)cobalt(II) were acquired from Sigma-Aldrich and dried prior to their use.

Inductively Coupled Plasma−Optical Emission Spectroscopy. The Sn at. % of the FITO nanocubes was determined using inductively coupled plasma−optical emission spectroscopy (ICP-OES) on a Varian 720-ES ICP optical emission spectrometer. NCs were digested with aqua regia (a 3:1 ratio mixture of 35% HCl and 70% HNO$_3$) and then diluted with Milli-Q water such that the total acid concentration is approximately 2 vol %. In and Sn standard solutions were prepared with variable concentrations by diluting commercially available ICP-OES standards with 2% HNO$_3$ solution in Milli-Q water.

Electron Microscopy. FITO NCs were imaged using a Hitachi S5500 scanning transmission electron microscope (STEM) operating in bright field mode at an accelerating voltage of 30 kV. The sizes of the NCs were found using ImageJ to determine a histogram of NC sizes for at least 150 particles and then fitting that distribution to a Gaussian.

Refractive Index Sensitivity. Extinction spectra were collected using an Agilent Cary 5000 UV−vis−NIR spectrophotometer. To determine the refractive index sensitivity (RIS), the NC optical extinction was measured for FITO NCs in hexane, chloroform, and tetrachloroethylene. The latter two solvent dispersions were prepared by precipitating the NCs using ethanol and then dispersing them in the new solvent. The extinction was measured on 9 serial dilutions for each solvent to check for signs of aggregation and establish error bars.

Reductive Titration. For the chemical reduction of FITO NCs, a 2 mM CoCp$_2$* solution in a 1:1 mixture of tetrahydrofuran (THF) and toluene was prepared along with a 0.02 M [H(OEt$_2$)]$^+$[BAr$_4^F$]$^−$ acid solution in a 1:2 mixture of oleic acid and THF. FITO NCs were precipitated from a stock solution in hexane using ethanol and then redispersed in a 1:1 THF/hexane mixture inside an Ar-filled glovebox. 50 μL of 0.02 M [H(OEt$_2$)]$^+$[BAr$_4^F$]$^−$ was added to 200 μL of the NC solution in a 1 mm path length quartz cuvette. This solution was titrated with 5 μL aliquots of 2 mM CoCp$_2$*, shaking the cuvette after every aliquot to ensure mixing. After waiting 1 min to ensure the sample had reached equilibrium, the optical extinction was measured using a fiber-coupled ASD Inc. PANalytical spectrometer.

Simulation Details. Theoretical optical extinction and electric field intensity maps were simulated using the COMSOL Wave Optics Module 6.0. A nanocube was simulated using a Drude dielectric function:

$$\varepsilon(\omega) = \varepsilon_\infty - \frac{\varepsilon_0 \omega_p^2}{\omega^2 + i\gamma\omega} \tag{1}$$

with ε_0 being the permittivity of free space and ε_∞ set to 4. Damping, γ, was set to 1000 cm^{-1}, and the bulk plasma frequency, ω_p, was varied between 12000 and 16000 cm^{-1}, consistent with previous estimates of the dielectric function of FITO.[32] The edges of the cube were rounded with a radius of curvature equal to 10% of the NC edge length to approximate the shapes observed by electron microscopy.

Surface depletion was incorporated into simulations by solving Poisson's equation using the COMSOL AC/DC Wave Optics Module 6.0 using the dimensionless form of Poisson's equation derived by Seiwatz and Green,[35] as previously done
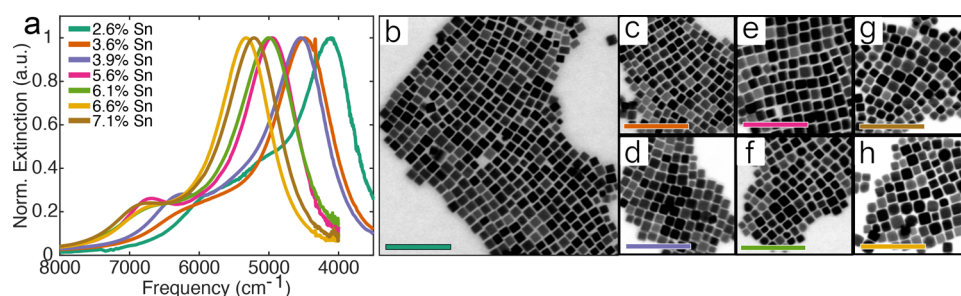
Figure 1. Fluorine and tin codoped indium oxide nanocubes. (a) Normalized optical extinction of NCs dispersed in hexane. (b−h) STEM micrographs of NCs doped with 2.6, 3.6, 3.9, 5.6, 6.1, 6.6, and 7.1 Sn at. %, respectively. Scale bars are 100 nm.
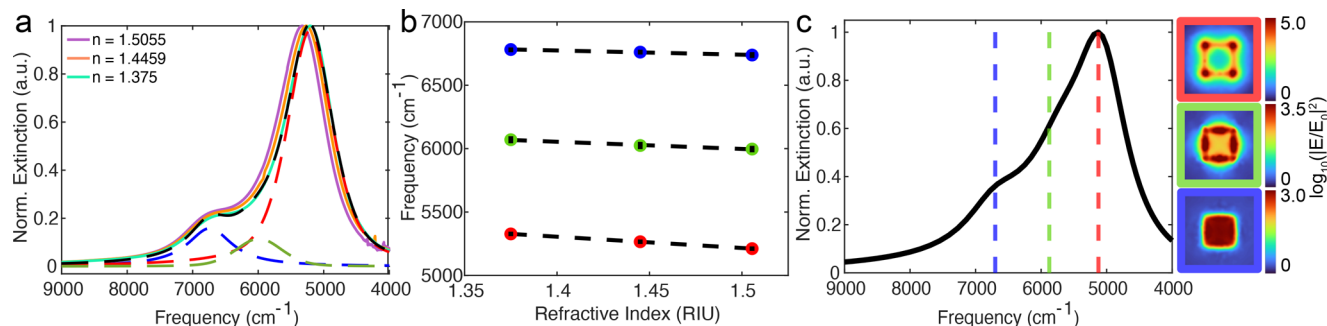

Figure 2. Refractive index sensitivity of 6.6 Sn at. % FITO NC multimodal plasmon absorption. Red, green, and blue refer to the corner, edge, and face mode, respectively (a) Normalized extinction (solid lines) of sample dispersed in hexane (n = 1.375), chloroform (n = 1.446), and tetrachloroethylene (n = 1.5055). Dashed lines show the deconvoluted LSPR modes (red, blue, and green) and the sum of these fits (black) for the sample dispersed in hexane. (b) Deconvoluted peak position versus solvent refractive index. Error bars are smaller than the data point size. The dashed black lines are linear fits. (c) Simulated optical extinction spectrum (left) and logarithmic normalized electric field maps (right) for the corner (red), edge (green), and face (blue) modes.

to simulate the effects of surface depletion in spherical ITO NCs.[30,36] The surface potential was set to 2.2 eV (referenced to the center of the bandgap), and the activated donor density was varied between $(0.65-1.01) \times 10^{21}$ cm^{-3}, corresponding to ω_p = 12000−15000 cm^{-1}. The optical extinction was then calculated using a Drude dielectric function with $\omega_p = \sqrt{n_e e^2/m_e \varepsilon_0}$, where m_e is the electron effective mass (set to 0.4), e is the charge on an electron, and n_e is the spatially varying free electron density determined by solving Poisson's equation.

RESULTS AND DISCUSSION

To investigate the role of faceting on the dielectric sensitivity of plasmonic metal oxide NCs, we synthesized a series of FITO nanocubes with varying Sn at. % (Figure 1). As previously reported,[25,32] fluorine induces faceting of indium oxide NPs by lowering the surface energy of the {100} facets, making them prevalent in the synthesized morphology and producing nanocubes with a multimodal LSPR in the near-infrared region. The LSPR frequency depends on n_e, which changes with the Sn dopant concentration—here, varied from 2.6 to 7.1% of the total cations, as determined by ICP-OES. The cubic morphology is maintained across the Sn incorporation range, as is evidenced by the multimodal LSPR optical extinction (Figure 1a) and by STEM (Figure 1b−h). The sizes and exact Sn at. % values are listed in Table S1.

A common metric for plasmonic sensing is refractive index sensitivity (RIS), which is defined as the change in the LSPR frequency (ω_{LSPR}) for a given change in the surrounding refractive index (n).

$$RIS = \frac{\Delta \omega_{LSPR}}{\Delta n} \tag{2}$$

This sensitivity is related to the strength of the plasmonic NFE within the surrounding dielectric medium, with sharp corners or edges both expected to result in higher NFE and higher RIS.[7,29,37] On the other hand, surface depletion has been shown to decrease RIS of ITO NCs, especially for smaller NCs and low Sn at. %, by decreasing the plasmonic volume fraction and effectively insulating that plasmonic volume from its dielectric environment.[30] Finite element simulations of FITO nanocubes predict an increased plasmonic NFE around the sharp nanocube edges and corners,[25] suggesting the associated plasmonic modes may also be more sensitive to changes in the dielectric environment. It is unclear how surface depletion might impact these modes; however, the impact on both effects is expected to be correlated: a greater depletion width is expected to decrease both the RIS and NFE.

To investigate the role that faceting and surface depletion have on RIS, seven FITO samples with Sn at. % ranging from 2.6% to 7.1% were dispersed in hexane (n = 1.375), chloroform (n = 1.446), and tetrachloroethylene (n = 1.5055), and the optical extinction of each dispersion was collected at nine different concentrations. The three peaks that contribute to the FITO optical extinction were deconvoluted using a linear combination of three pseudo-Voigt functions (Figures 2a and S1 and Table S1), and the RIS was extracted using a linear fit to the peak positions versus refractive index (Figures 2b and S2 and Table S2), using the different concentrations to establish error bars. The envelope of the spectral line shape was found to change with n as a result of different peak shifts for each component mode, discovered upon deconvolution. Each

sample, thus, has three distinct sensitivities—one associated with each of the three LSPR modes.
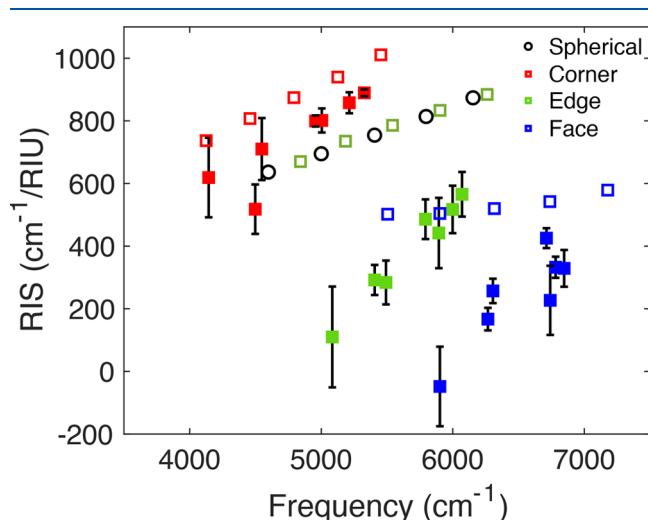

Figure 3. Comparison of simulated (open points) and experimental (filled points) refractive index sensitivity for a series of FITO NCs with different Sn at. %. The simulations assume a uniform free electron density distribution. The resonant frequency (*x*-axis) for each data point is for a medium refractive index of 1.375, corresponding to NCs dispersed in hexane.

Concurrently, COMSOL was used to carry out finite element method (FEM) simulations to compute the theoretical RIS of nanocubes with variable free electron density. The Drude−Lorentz model was used to describe the nanocube dielectric function, with the bulk plasma frequency ranging from 12000 to 16000 cm^{-1} and a damping constant of 1000 cm^{-1}, which is in line with previous estimates of the FITO dielectric function.[25] Consistent with previous studies of plasmonic nanocubes, FEM field intensity maps show that the three modes observed in the spectral line shape correspond to dipolar resonances associated with the corners, edges, and faces (Figure 2c)[25,38] with the surface charge distribution consistent with three of the six main bright resonances that have been calculated for nanocubes (Figure S3).[39−41] Mimicking the experimental measurements, the refractive index of the nanocube surroundings was systematically varied, the three optical extinction peaks were deconvoluted (Figure S4 and Table S3), and a linear fit was used to determine the theoretical RIS (Figure S5 and Table S4). For comparison, the

same dielectric function was used to calculate the theoretical RIS of a nanosphere.

There is a direct correlation between an LSPR mode's resonant frequency and its dielectric sensitivity.[16,42,43] Overlaid on this trend, shape has a significant effect by influencing the polarizability and NFE of the LSPR mode, both positively correlated to higher RIS.[7,17,21] To understand how the faceting of FITO nanocubes impacts dielectric sensitivity, the RIS of each of the three modes was examined as a function of LSPR resonant frequency (Figure 3), comparing the experimentally measured values to those predicted through simulation. While RIS is most commonly reported in units of wavelength (nm/RIU), we instead opt to use wavenumbers (cm^{-1}/RIU). With variable Sn at. %, the FITO LSPR spans a very wide wavelength range of ~1000 nm, and the nonlinear relationship between wavelength and energy causes an apparent reversal of the dependence of RIS on energy for high energy (edge and face) versus lower energy (corner) modes, obfuscating the underlying physics (Figure S6). When the sensitivity is plotted on a linear energy scale instead (here, in units of wavenumbers), the observed trends in sensitivity are consistent across all three modes, as expected given the aforementioned relationship between LSPR resonant frequency and sensitivity.[42]

Looking first at the theoretical RIS, the sensitivity of the modes follows the same trend as the simulated field enhancement—the corner mode is the most sensitive, followed by the edge and then the face mode. Considering a resonance of ~5500 cm^{-1}, for example, the corner mode is predicted to be about twice as sensitive as the face mode and ~30% more sensitive than the edge mode or the spherical case. Comparing simulations to experimental results, the corner mode remains the most sensitive, albeit slightly less sensitive than simulations predict. Greater quantitative discrepancies between simulation and experiment arise, however, with the RIS of the edge and face modes. Both are substantially less sensitive than predicted. In addition, the difference between the theoretical and experimental sensitivity widens for the samples with the lowest Sn at. % (i.e., lower resonant frequency). Notably, the surface depletion width expands for lower Sn at. % in ITO NCs,[30,31] so we hypothesized that the lower than predicted FITO nanocube RIS may be due to the impact of surface depletion, which was not accounted for in the simulations.

The spectral response of plasmonic metal oxide NCs can be modified by postsynthetic charging through chemical reduction.[44−47] Reducing agents transfer electrons to metal oxide NCs by proton-coupled electron transfer, and the resulting
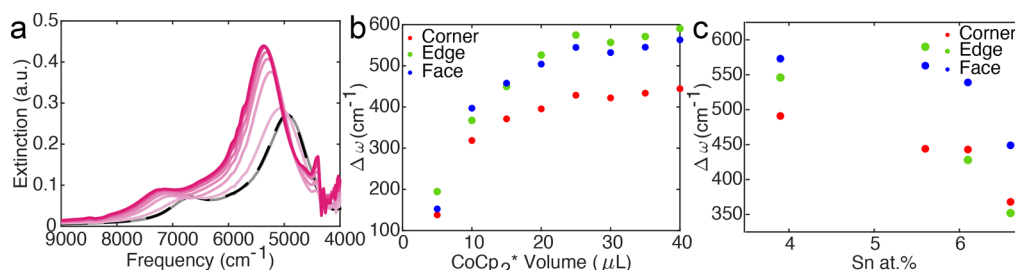

Figure 4. Reductive chemical modulation of FITO nanocube LSPR. (a) Extinction of a 5.6 at. % Sn FITO NC dispersion during titration with 2 mM CoCp$_2$*. The gray solid curve is the initial NC dispersion, and the black dashed line is after adding [H(OEt$_2$)]$^+$[BAr$_4^F$]$^-$. Darkening shades of magenta show increasing amounts of added CoCp$_2$*. (b) Deconvoluted peak position versus added volume of 2 mM CoCp$_2$*. (c) Maximum LSPR shift versus Sn at. %.
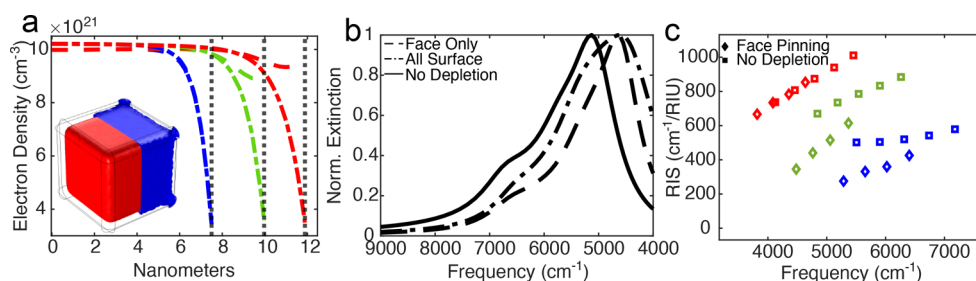
Figure 5. LSPR simulations incorporating surface depletion. (a) 1-D electron density profiles moving from the center of the cube to the corner (red), edge center (green), and face center (blue). The dashed lines reflect a surface potential set to 2.2 eV at the faces only, and the dashed and dotted curves reflect a surface potential set to 2.2 eV across the entire surface. The dotted black line indicates the surface of the nanocube along each 1-D profile. The inset shows an electron density isosurface for 9×10^{20} cm^{-3} for the case where the Fermi level is pinned at the faces only (blue) and when the Fermi level is pinned across the entire nanocube surface (red). (b) Simulated extinction of FITO nanocubes with a donor density of 10.1×10^{21} cm^{-3}. The solid curve is in the absence of surface depletion, the dashed curve is for the surface potential set to 2.2 eV at the faces only, and the dashed and dotted curve is for the surface potential set to 2.2 eV across the entire surface. 2.2 eV was chosen for the resulting line shape's qualitative agreement with experiment. (c) Comparison of the simulated refractive index sensitivity versus resonant frequency for the case with no surface depletion (squares) and with a 2.2 eV surface potential on the faces only (diamonds). Red, green, and blue are the corner, edge, and face modes, respectively.

increase in free electron concentration blue-shifts the LSPR resonant frequency until a saturation point, beyond which additional reducing agent no longer shifts the LSPR. The maximum modulation for a given NC sample depends on the initial spatial distribution of free electrons, with a larger depletion width resulting in a higher maximum modulation of the LSPR frequency.[48] Because surface depletion strongly influences the spectral response of ITO NCs to electron accumulation by postsynthetic charging,[30,36,48,49] we performed a series of reductive titration experiments on FITO nanocubes.

To probe the impact of depletion on the multimodal FITO NC LSPR, we titrated NC dispersions in a 1:1 solution of hexane and THF with the reducing agent decamethylcobaltocene (CoCp$_2$*), with [H(OEt$_2$)]$^+$[BAr$_4^F$]$^-$ included as a proton source for charge balance. Aliquots were added until the LSPR stopped shifting, and then the spectra were deconvoluted to determine the extent of modulation for each of the three modes (Figures 4 and S7). Within instrumental limitations, we were able to compare trends for chemical modulation for nanocubes with Sn at. % ranging from 3.87 to 6.63% (Figure 4c). Across all samples, the face mode is modulated to the greatest extent, and the corner mode is modulated to a lesser extent. The modulation in the edge mode depends on Sn at. %, shifting by a much greater extent for samples with lower Sn at. %. Across all modes, lower Sn at. % is correlated to greater modulation.

Hence, LSPR modulation trends are the reverse of trends in RIS when evaluating their variation with LSPR mode and with Sn at. %. This inverse relationship supports the hypothesis that surface depletion is responsible for the observed trends in experimental RIS and its deviation from theoretical predictions. The corner mode is modulated less by chemical reduction, indicating a smaller depletion width insulating that mode from the local dielectric environment. As such, it retains a high sensitivity across all samples—close to the values predicted through simulations. The face and edge modes, on the other hand, are more strongly modulated by chemical reduction, indicating a greater influence of surface depletion, which insulates those modes from the local dielectric environment lowering their RIS compared to theoretical predictions.

The differential impact of surface depletion on different geometric modes emerges uniquely in FITO nanocubes, where the distinct chemistry and electronic structure of the surface terminations contrast with the isotropic depletion of ITO NCs. The corner mode, which gives rise to the strongest extinction, the highest NFE, and greatest RIS, also appears to be the least affected by surface depletion. The proximity of its experimental RIS to the values predicted in the absence of depletion suggests that FITO nanocubes experience spatially nonuniform Fermi level pinning across their surfaces. To explore the impact of facet-dependent Fermi level pinning on the RIS of each mode, we incorporated a nonuniform charge density into our FEM simulations. Poisson's equation was solved for a cube with a given surface potential, and the resulting free electron density distribution was used to calculate the NC optical extinction. Two cases were explored: pinning the Fermi level uniformly across the entire NC surface and pinning the Fermi level on only the faces of the cube. In the former case, a depletion layer forms near the entire nanocube surface, shrinking the plasmonic volume to a rounded cubic region within the physical boundaries of the nanocube. In the latter case, the surface depletion width is nonuniform, as the free electron density is less impacted near the edges and corners (Figure 5a). To help visualize the influence of Fermi level pinning on the plasmonic volume, the inset to Figure 5a shows the isosurfaces for a free electron density of 9×10^{20} cm^{-3}. The red half of the isosurface has the Fermi level pinned across the entire surface, while the blue half of the isosurface has the Fermi level pinned only on the faces of the cube. This particular free electron density was chosen as it best highlights the difference between the two cases, though similar shapes occur for isosurfaces at other values of the electron density. Contrasting with the rounded corners of the plasmonic volume for uniform Fermi level pinning, the free electron density remains high near the corners of the cube if the Fermi level is only pinned only at the cube faces.

The difference in free electron density distribution changes the optical extinction line shapes for the two hypothetical Fermi level pinning scenarios (Figure 5b). Any amount of depletion red-shifts the LSPR, likely due to the surface depletion width acting as a high dielectric constant shell around the plasmonic volume. Qualitatively, however, the spectrum with Fermi level pinning only on the nanocube faces

is a closer match to the experimentally observed line shape: the face mode decreases in intensity compared to the case without depletion, but the overall line shape remains similar. In contrast, with Fermi level pinning over the entire nanocube surface, the corner mode shows a decreased contribution to the extinction, and the edge mode has a much larger overall contribution to the line shape than is observed experimentally; these two components become comparable in intensity, leading to a broad peak maximum not seen in experiments. The resemblance of the face-only Fermi level pinning spectrum to the experimental results is reinforced by the ability of this model to reproduce the experimental trends for dielectric sensitivity of the three LSPR modes (Figures 5c, S8, and S9). The edge and face modes have lower sensitivity compared to the case with no surface depletion, especially at lower resonant frequencies (i.e., lower Sn at. %), while the corner mode retains the same sensitivity. The hypothetical case of uniform Fermi level pinning failed to reproduce these RIS trends, even suggesting that the RIS of each mode should decrease with higher resonant frequency (Figure S10).

These simulation results, combined with the trends in LSPR modulation by reductive titration, give a consistent picture of the mode-dependent impact of FITO nanocube surface depletion. Fermi level pinning occurs predominantly on the faces of FITO nanocubes, and the depletion width extends into the nanocube radially from the faces. The face mode, thus, decreases in its sensitivity, being the mode most insulated from its dielectric environment, while the corner mode retains its sensitivity as the depletion width does not significantly impinge on the electron density near the cube corners. While the Fermi level is not specifically pinned at the edges of the nanocube, the depletion width extending from the faces nonetheless insulates the edge mode somewhat from its dielectric environment, and depletion impacts the edge mode more severely for low Sn at. %. As a result, the edge mode RIS decreases to a much greater extent with frequency than does the face mode, and in the reductive titrations the edge mode modulation is comparable with the face mode in lower Sn at. % samples, while it is comparable with the corner mode for higher Sn at. % samples.

The physical origins of this apparent facet-specific Fermi level pinning can likely be traced to differences in the energies and prevalence of surface states. Surface states in metal oxides are understood to be associated with surface-adsorbed hydroxyls.[50−54] The density of surface states and the resulting Fermi level pinning are, thus, dependent on the surface binding preference of hydroxyls. This behavior has been well documented, for example, in ZnO, where the polarity of the exposed facet influences the surface hydroxyl coverage and resulting Fermi level pinning.[53,54] Similarly for indium oxide, recent DFT studies have predicted that hydroxyls adsorb more strongly to the (211) facet of indium oxide than they do to the (111) facet.[55] In addition, hydroxyl termination is understood to stabilize the {100} facets of In_2O_3 NCs, leading to a cubic morphology.[56] It is likely that the predominance of Fermi level pinning along the faces of the FITO nanocube as opposed to the edges and corners is due to differences in the density of surface states brought about by differences in hydroxylation of the exposed facet.

CONCLUSIONS AND OUTLOOK

In conclusion, we showed that the faceting of FITO nanocubes increases the dielectric sensitivity of the corner mode above that of spherical NCs with the same material properties. That

said, the FITO NC LSPR sensitivity is lower than expected based on simulations, a result that we attribute to the surface trapping of free electrons leading to a depletion region that insulates the plasmonic volume from its dielectric environment. We provide support for this hypothesis using reductive chemical modulation of the LSPR, showing that lower Sn at. % is correlated to a greater extent of modulation and that the mode-dependent dielectric sensitivity is anticorrelated to a mode-dependent extent of LSPR modulation during reduction. To confirm this interpretation, we incorporate surface depletion into FEM optical simulations by solving Poisson's equation and then using the resulting free electron density distribution to simulate the optical extinction. Through these surface depletion simulations, we show that the trend in sensitivity can be best explained by Fermi level pinning on the faces of the nanocube, which insulates both the face and the edge modes from their local dielectric environment while leaving the corner mode largely unaffected. These results show that the corner mode is the most viable for sensing applications, as it has the highest extinction and sensitivity across all samples, and that higher dopant incorporation leads to higher sensitivity. The ideal FITO NC sample for dielectric sensing or other applications driven by high NFE is therefore one with both a high degree of faceting and a greater amount of Sn incorporation.

The mode-dependent impact of the surface depletion revealed through this study indicates that the corners of FITO nanocubes provide the best opportunity for plasmonic enhancement of molecular spectroscopic signatures, through both the high NFE inherent to the sharp faceting and, strikingly, the reduced impact of the surface depletion layer on the LSPR mode associated with the nanocube corners. Molecules bound to the corners, as opposed to the faces of the nanocube, are likely to have the greatest impact on the LSPR resonant frequency through the resulting high corner-mode dielectric sensitivity. Beyond just dielectric sensitivity, however, the high field enhancement and the decreased impact of surface depletion around the corners of the nanocubes may make FITO NCs ideal for IR sensing applications utilizing plasmonic enhancement of molecular spectroscopic signatures, such as surface-enhanced Raman spectroscopy[57,58] and infra-red absorption.[9,28,59] Indeed, the direct coupling of oleate molecular vibrational modes to LSPR modes of rounded FITO nanocubes has been previously reported,[14] specifically taking advantage of the tunable overlap of the FITO LSPR with molecular vibrational modes in the mid-infrared region. In addition, the spatial variation in NFE may provide an opportunity for plasmon-driven spatially localized chemistry, leveraging the high electric field and low surface depletion width at the corners of the FITO nanocube to create a "chemical hot spot".[60−63]

■ ASSOCIATED CONTENT

ⓢ Supporting Information

The Supporting Information is available free of charge at https://pubs.acs.org/doi/10.1021/acs.jpcc.2c08495.

Additional materials characterization, example spectral deconvolutions, and additional simulations (PDF)

■ AUTHOR INFORMATION

Corresponding Author

Delia J. Milliron − *McKetta Department of Chemical Engineering, University of Texas at Austin, Austin, Texas 78712, United States; Department of Chemistry, University of Texas at Austin, Austin, Texas 78712, United States;* ⦿ orcid.org/0000-0002-8737-451X; Email: milliron@che.utexas.edu

Authors

Benjamin J. Roman − *McKetta Department of Chemical Engineering, University of Texas at Austin, Austin, Texas 78712, United States;* ⦿ orcid.org/0000-0003-2213-2533

Sofia A. Shubert-Zuleta − *Department of Chemistry, University of Texas at Austin, Austin, Texas 78712, United States;* ⦿ orcid.org/0000-0003-0445-175X

Grant Shim − *McKetta Department of Chemical Engineering, University of Texas at Austin, Austin, Texas 78712, United States*

Victoria Kyveryga − *McKetta Department of Chemical Engineering, University of Texas at Austin, Austin, Texas 78712, United States;* ⦿ orcid.org/0000-0003-1624-4897

Mohamed Faris − *McKetta Department of Chemical Engineering, University of Texas at Austin, Austin, Texas 78712, United States*

Complete contact information is available at:
https://pubs.acs.org/10.1021/acs.jpcc.2c08495

Notes

The authors declare no competing financial interest.

■ REFERENCES

(1) McFarland, A. D.; Van Duyne, R. P. Single Silver Nanoparticles as Real-Time Optical Sensors with Zeptomole Sensitivity. *Nano Lett.* **2003**, *3*, 1057−1062.

(2) Anker, J. N.; Hall, W. P.; Lyandres, O.; Shah, N. C.; Zhao, J.; Van Duyne, R. P. Biosensing with Plasmonic Nanosensors. *Nat. Mater.* **2008**, *7*, 442−453.

(3) Mayer, K. M.; Hafner, J. H. Localized Surface Plasmon Resonance Sensors. *Chem. Rev.* **2011**, *111*, 3828−3857.

(4) Versiani, A. F.; Martins, E. M. N.; Andrade, L. M.; Cox, L.; Pereira, G. C.; Barbosa-Stancioli, E. F.; Nogueira, M. L.; Ladeira, L. O.; da Fonseca, F. G. Nanosensors Based on LSPR Are Able to Serologically Differentiate Dengue from Zika Infections. *Sci. Rep.* **2020**, *10*, 11302.

(5) Chen, P.; Chung, M. T.; McHugh, W.; Nidetz, R.; Li, Y.; Fu, J.; Cornell, T. T.; Shanley, T. P.; Kurabayashi, K. Multiplex Serum Cytokine Immunoassay Using Nanoplasmonic Biosensor Microarrays. *ACS Nano* **2015**, *9*, 4173−4181.

(6) Hong, Y.; Ku, M.; Lee, E.; Suh, J.-S.; Huh, Y.-M.; Yoon, D. S.; Yang, J. Localized Surface Plasmon Resonance Based Nanobiosensor for Biomarker Detection of Invasive Cancer Cells. *J. Biomed. Opt.* **2014**, *19*, 051202.

(7) Hooshmand, N.; Bordley, J. A.; El-Sayed, M. A. Plasmonic Spectroscopy: The Electromagnetic Field Strength and Its Distribution Determine the Sensitivity Factor of Face-to-Face Ag Nanocube Dimers in Solution and on a Substrate. *J. Phys. Chem. C* **2015**, *119*, 15579−15587.

(8) Stiles, P. L.; Dieringer, J. A.; Shah, N. C.; Van Duyne, R. P. Surface-Enhanced Raman Spectroscopy. *Annual Rev. Anal. Chem.* **2008**, *1*, 601−626.

(9) Abb, M.; Wang, Y.; Papasimakis, N.; de Groot, C. H.; Muskens, O. L. Surface-Enhanced Infrared Spectroscopy Using Metal Oxide Plasmonic Antenna Arrays. *Nano Lett.* **2014**, *14*, 346−352.

(10) Jaque, D.; Martínez Maestro, L.; del Rosal, B.; Haro-Gonzalez, P.; Benayas, A.; Plaza, J. L.; Martín Rodríguez, E.; García Solé, J. Nanoparticles for Photothermal Therapies. *Nanoscale* **2014**, *6*, 9494−9530.

(11) Zhang, H.; Govorov, A. O. Optical Generation of Hot Plasmonic Carriers in Metal Nanocrystals: The Effects of Shape and Field Enhancement. *J. Phys. Chem. C* **2014**, *118*, 7606−7614.

(12) Brongersma, M. L.; Halas, N. J.; Nordlander, P. Plasmon-Induced Hot Carrier Science and Technology. *Nat. Nanotechnol.* **2015**, *10*, 25−34.

(13) Adato, R.; Artar, A.; Erramilli, S.; Altug, H. Engineered Absorption Enhancement and Induced Transparency in Coupled Molecular and Plasmonic Resonator Systems. *Nano Lett.* **2013**, *13*, 2584−2591.

(14) Agrawal, A.; Singh, A.; Yazdi, S.; Singh, A.; Ong, G. K.; Bustillo, K.; Johns, R. W.; Ringe, E.; Milliron, D. J. Resonant Coupling between Molecular Vibrations and Localized Surface Plasmon Resonance of Faceted Metal Oxide Nanocrystals. *Nano Lett.* **2017**, *17*, 2611−2620.

(15) Peng, S.; Du, C.; Shi, D. Geometry and Near-Field Coupling Effects on the Refractive-Index Sensitivities of Individual Ag Nanoparticle Sensors. *Appl. Phys. A: Mater. Sci. Process.* **2017**, *123*, 672.

(16) Khan, A. U.; Zhao, S.; Liu, G. Key Parameter Controlling the Sensitivity of Plasmonic Metal Nanoparticles: Aspect Ratio. *J. Phys. Chem. C* **2016**, *120*, 19353−19364.

(17) Chen, H.; Kou, X.; Yang, Z.; Ni, W.; Wang, J. Shape- and Size-Dependent Refractive Index Sensitivity of Gold Nanoparticles. *Langmuir* **2008**, *24*, 5233−5237.

(18) Lee, K.-S.; El-Sayed, M. A. Gold and Silver Nanoparticles in Sensing and Imaging: Sensitivity of Plasmon Response to Size, Shape, and Metal Composition. *J. Phys. Chem. B* **2006**, *110*, 19220−19225.

(19) Lu, L.-y.; Zhu, J.; Weng, G.-j.; Li, J.-J.; Zhao, J.-W. Plasmonic Refractive Index Sensitivity of Tetrapod Gold Nanostars: Tuning the Branch Length and Protein Layer. *Eur. Phys. J. D* **2022**, *76*, 54.

(20) Luo, X.; Qiao, L.; Xia, Z.; Yu, J.; Wang, X.; Huang, J.; Shu, C.; Wu, C.; He, Y. Shape- and Size-Dependent Refractive Index Sensing and SERS Performance of Gold Nanoplates. *Langmuir* **2022**, *38*, 6454−6463.

(21) Chen, H.; Shao, L.; Woo, K. C.; Ming, T.; Lin, H.-Q.; Wang, J. Shape-Dependent Refractive Index Sensitivities of Gold Nanocrystals with the Same Plasmon Resonance Wavelength. *J. Phys. Chem. C* **2009**, *113*, 17691−17697.

(22) Agrawal, A.; Cho, S. H.; Zandi, O.; Ghosh, S.; Johns, R. W.; Milliron, D. J. Localized Surface Plasmon Resonance in Semiconductor Nanocrystals. *Chem. Rev.* **2018**, *118*, 3121−3207.

(23) Kriegel, I.; Scotognella, F.; Manna, L. Plasmonic Doped Semiconductor Nanocrystals: Properties, Fabrication, Applications and Perspectives. *Phys. Rep.* **2017**, *674*, 1−52.

(24) Staller, C. M.; Gibbs, S. L.; Saez Cabezas, C. A.; Milliron, D. J. Quantitative Analysis of Extinction Coefficients of Tin-Doped Indium Oxide Nanocrystal Ensembles. *Nano Lett.* **2019**, *19*, 8149−8154.

(25) Cho, S. H.; Roccapriore, K. M.; Dass, C. K.; Ghosh, S.; Choi, J.; Noh, J.; Reimnitz, L. C.; Heo, S.; Kim, K.; Xie, K.; et al. Spectrally Tunable Infrared Plasmonic F,Sn:In$_2$O$_3$ Nanocrystal Cubes. *J. Chem. Phys.* **2020**, *152*, 014709.

(26) Bukasov, R.; Shumaker-Parry, J. S. Silver Nanocrescents with Infrared Plasmonic Properties As Tunable Substrates for Surface

Enhanced Infrared Absorption Spectroscopy. *Anal. Chem.* **2009**, *81*, 4531−4535.

(27) Wu, C.; Khanikaev, A. B.; Adato, R.; Arju, N.; Yanik, A. A.; Altug, H.; Shvets, G. Fano-Resonant Asymmetric Metamaterials for Ultrasensitive Spectroscopy and Identification of Molecular Monolayers. *Nat. Mater.* **2012**, *11*, 69−75.

(28) Adato, R.; Aksu, S.; Altug, H. Engineering Mid-Infrared Nanoantennas for Surface Enhanced Infrared Absorption Spectroscopy. *Mater. Today* **2015**, *18*, 436−446.

(29) Agrawal, A.; Kriegel, I.; Milliron, D. J. Shape-Dependent Field Enhancement and Plasmon Resonance of Oxide Nanocrystals. *J. Phys. Chem. C* **2015**, *119*, 6227−6238.

(30) Zandi, O.; Agrawal, A.; Shearer, A. B.; Reimnitz, L. C.; Dahlman, C. J.; Staller, C. M.; Milliron, D. J. Impacts of Surface Depletion on the Plasmonic Properties of Doped Semiconductor Nanocrystals. *Nat. Mater.* **2018**, *17*, 710−717.

(31) Gibbs, S. L.; Staller, C. M.; Milliron, D. J. Surface Depletion Layers in Plasmonic Metal Oxide Nanocrystals. *Acc. Chem. Res.* **2019**, *52*, 2516−2524.

(32) Cho, S. H.; Ghosh, S.; Berkson, Z. J.; Hachtel, J. A.; Shi, J.; Zhao, X.; Reimnitz, L. C.; Dahlman, C. J.; Ho, Y.; Yang, A.; et al. Syntheses of Colloidal F:In$_2$O$_3$ Cubes: Fluorine-Induced Faceting and Infrared Plasmonic Response. *Chem. Mater.* **2019**, *31*, 2661−2676.

(33) Ye, X.; Fei, J.; Diroll, B. T.; Paik, T.; Murray, C. B. Expanding the Spectral Tunability of Plasmonic Resonances in Doped Metal-oxide Nanocrystals through Cooperative Cation−Anion Codoping. *J. Am. Chem. Soc.* **2014**, *136*, 11680−11686.

(34) Runnerstrom, E. L.; Kelley, K. P.; Sachet, E.; Shelton, C. T.; Maria, J.-P. Epsilon-near-zero Modes and Surface Plasmon Resonance in Fluorine-doped Cadmium Oxide Thin Films. *ACS Photonics* **2017**, *4*, 1885−1892.

(35) Seiwatz, R.; Green, M. Space Charge Calculations for Semiconductors. *J. Appl. Phys.* **1958**, *29*, 1034−1040.

(36) Agrawal, A.; Kriegel, I.; Runnerstrom, E. L.; Scotognella, F.; Llordes, A.; Milliron, D. J. Rationalizing the Impact of Surface Depletion on Electrochemical Modulation of Plasmon Resonance Absorption in Metal Oxide Nanocrystals. *ACS Photonics* **2018**, *5*, 2044−2050.

(37) Haes, A. J.; Zou, S.; Schatz, G. C.; Van Duyne, R. P. A Nanoscale Optical Biosensor: The Long Range Distance Dependence of the Localized Surface Plasmon Resonance of Noble Metal Nanoparticles. *J. Phys. Chem. B* **2004**, *108*, 109−116.

(38) Nicoletti, O.; de la Peña, F.; Leary, R. K.; Holland, D. J.; Ducati, C.; Midgley, P. A. Three-Dimensional Imaging of Localized Surface Plasmon Resonances of Metal Nanoparticles. *Nature* **2013**, *502*, 80−84.

(39) Cortie, M. B.; Liu, F.; Arnold, M. D.; Niidome, Y. Multimode Resonances in Silver Nanocuboids. *Langmuir* **2012**, *28*, 9103−9112.

(40) Tzarouchis, D.; Ylä-Oijala, P.; Sihvola, A. Subwavelength Hexahedral Plasmonic Scatterers: History, Symmetries, and Resonant Characteristics. *Photonics* **2019**, *6*, 18.

(41) Klimov, V.; Guo, G.-Y.; Pikhota, M. Plasmon Resonances in Metal Nanoparticles with Sharp Edges and Vertices: A Material Independent Approach. *J. of Phys. Chem. C* **2014**, *118*, 13052−13058.

(42) Miller, M. M.; Lazarides, A. A. Sensitivity of Metal Nanoparticle Surface Plasmon Resonance to the Dielectric Environment. *J. Phys. Chem. B* **2005**, *109*, 21556−21565.

(43) Saison-Francioso, O.; Lévêque, G.; Boukherroub, R.; Szunerits, S.; Akjouj, A. Dependence between the Refractive-Index Sensitivity of Metallic Nanoparticles and the Spectral Position of Their Localized Surface Plasmon Band: A Numerical and Analytical Study. *J. Phys. Chem. C* **2015**, *119*, 28551−28559.

(44) Valdez, C. N.; Schimpf, A. M.; Gamelin, D. R.; Mayer, J. M. Proton-controlled Reduction of ZnO Nanocrystals: Effects of Molecular Reductants, Cations, and Thermodynamic Limitations. *J. Am. Chem. Soc.* **2016**, *138*, 1377−1385.

(45) Valdez, C. N.; Braten, M.; Soria, A.; Gamelin, D. R.; Mayer, J. M. Effect of Protons on the Redox Chemistry of Colloidal Zinc Oxide Nanocrystals. *J. Am. Chem. Soc.* **2013**, *135*, 8492−8495.

(46) Valdez, C. N.; Delley, M. F.; Mayer, J. M. Cation Effects on the Reduction of Colloidal ZnO Nanocrystals. *J. Am. Chem. Soc.* **2018**, *140*, 8924−8933.

(47) Schimpf, A. M.; Knowles, K. E.; Carroll, G. M.; Gamelin, D. R. Electronic Doping and Redox-Potential Tuning in Colloidal Semiconductor Nanocrystals. *Acc. Chem. Res.* **2015**, *48*, 1929−1937.

(48) Tandon, B.; Shubert-Zuleta, S. A.; Milliron, D. J. Investigating the Role of Surface Depletion in Governing Electron-Transfer Events in Colloidal Plasmonic Nanocrystals. *Chem. Mater.* **2022**, *34*, 777−788.

(49) Ghini, M.; Curreli, N.; Lodi, M. B.; Petrini, N.; Wang, M.; Prato, M.; Fanti, A.; Manna, L.; Kriegel, I. Control of Electronic Band Profiles through Depletion Layer Engineering in Core−Shell Nanocrystals. *Nat. Commun.* **2022**, *13*, 537.

(50) Ephraim, J.; Lanigan, D.; Staller, C.; Milliron, D. J.; Thimsen, E. Transparent Conductive Oxide Nanocrystals Coated with Insulators by Atomic Layer Deposition. *Chem. Mater.* **2016**, *28*, 5549−5553.

(51) Gassenbauer, Y.; Schafranek, R.; Klein, A.; Zafeiratos, S.; Hävecker, M.; Knop-Gericke, A.; Schlögl, R. Surface States, Surface Potentials, and Segregation at Surfaces of Tin-doped In$_2$O$_3$. *Phys. Rev. B* **2006**, *73*, 245312.

(52) Thimsen, E.; Johnson, M.; Zhang, X.; Wagner, A. J.; Mkhoyan, K. A.; Kortshagen, U. R.; Aydil, E. S. High Electron Mobility in Thin Films Formed via Supersonic Impact Deposition of Nanocrystals Synthesized in Nonthermal Plasmas. *Nat. Commun.* **2014**, *5*, 1−9.

(53) Heinhold, R.; Williams, G. T.; Cooil, S. P.; Evans, D. A.; Allen, M. W. Influence of Polarity and Hydroxyl Termination on the Band Bending at ZnO Surfaces. *Phys. Rev. B* **2013**, *88*, 235315.

(54) Heinhold, R.; Cooil, S. P.; Evans, D. A.; Allen, M. W. Stability of the Surface Electron Accumulation Layers on the Nonpolar (10$\overline{1}$0) and (11$\overline{2}$0) Faces of ZnO. *J. Phys. Chem. C* **2014**, *118*, 24575−24582.

(55) Shan, N.; Jones, J. C.; Luo, C.; Hock, A. S.; Martinson, A. B. F.; Cheng, L. Selective Hydroxylation of In$_2$O$_3$ as A Route to Site-Selective Atomic Layer Deposition. *J. Phys. Chem. C* **2022**, *126*, 10359−10366.

(56) Jansons, A. W.; Hutchison, J. E. Continuous Growth of Metal Oxide Nanocrystals: Enhanced Control of Nanocrystal Size and Radial Dopant Distribution. *ACS Nano* **2016**, *10*, 6942−6951.

(57) Zhang, Q.; Li, X.; Ma, Q.; Zhang, Q.; Bai, H.; Yi, W.; Liu, J.; Han, J.; Xi, G. A Metallic Molybdenum Dioxide with High Stability for Surface Enhanced Raman Spectroscopy. *Nat. Commun.* **2017**, *8*, 1−9.

(58) Schatz, G. C. Theoretical Studies of Surface Enhanced Raman Scattering. *Acc. Chem. Res.* **1984**, *17*, 370−376.

(59) Neubrech, F.; Huck, C.; Weber, K.; Pucci, A.; Giessen, H. Surface-enhanced infrared spectroscopy using resonant nanoantennas. *Chem. Rev.* **2017**, *117*, 5110−5145.

(60) Gargiulo, J.; Berté, R.; Li, Y.; Maier, S. A.; Cortés, E. From Optical to Chemical Hot Spots in Plasmonics. *Acc. Chem. Res.* **2019**, *52*, 2525−2535.

(61) Zhan, C.; Chen, X.-J.; Yi, J.; Li, J.-F.; Wu, D.-Y.; Tian, Z.-Q. From Plasmon-enhanced Molecular Spectroscopy to Plasmon-mediated Chemical Reactions. *Nat. Rev. Chem.* **2018**, *2*, 216−230.

(62) Cortés, E.; Xie, W.; Cambiasso, J.; Jermyn, A. S.; Sundararaman, R.; Narang, P.; Schlücker, S.; Maier, S. A. Plasmonic Hot Electron Transport Drives Nano-localized Chemistry. *Nat. Commun.* **2017**, *8*, 1−10.

(63) Linic, S.; Christopher, P.; Xin, H.; Marimuthu, A. Catalytic and Photocatalytic Transformations on Metal Nanoparticles with Targeted Geometric and Plasmonic Properties. *Acc. Chem. Res.* **2013**, *46*, 1890−1899.